Polyhedron 29 (2010) 2696–2702

Contents lists available at ScienceDirect

Polyhedron

journal homepage: www.elsevier.com/locate/poly

Synthesis and characterization of rigid +2 and +3 heteroleptic dinuclear ruthenium(II) complexes

J.R. Alston, S. Kobayashi, T.J. Younts, J.C. Poler *

Chemistry Department, The University of North Carolina at Charlotte, 9201 University City Blvd., Charlotte, NC 28223, USA

ARTICLE INFO

Article history:
Received 30 April 2010
Accepted 18 June 2010
Available online 25 June 2010

Keywords:
Multinuclear
Coordination complex
Polypyridine ligand
Charge transfer
MLCT

ABSTRACT

Synthesis and characterization of the dinuclear ruthenium coordination complexes with heteroleptic ligand sets, $[Cl(terpy)Ru(tpphz)Ru(terpy)Cl](PF_6)_2$ **(7)** and $[(phen)_2Ru(tpphz)Ru(terpy)Cl](PF_6)_3$ **(8)**, are reported. Both structures contain a tetrapyrido[3,2-α:2′,3′-c:3″,2″-h:2″,3″-j]phenazine (tpphz) **(6)** ligand bridging the two metal centers. Complex **7** was obtained *via* ligand exchange between, $RuCl_2$-(terpy)DMSO **(5)** and a tpphz bridge. Complex **8** was obtained *via* ligand exchange between, $[Ru(phen)_2tpphz](PF_6)_2$ **(4)** and $RuCl_2$(terpy)DMSO **(5)**. Metal-to-ligand-charge-transfer (MLCT) absorptions are sensitive to ligand set composition and are significantly red-shifted due to more electron donating ligands. Complexes **7**–**9** have been characterized by analytical, spectroscopic (IR, NMR, and UV–Vis), and mass spectrometric techniques. The electronic spectral properties of **7**, **8**, and $[(phen)_2Ru(tpphz)$-$Ru(phen)_2](PF_6)_4$ **(9)**, a previously reported +4 analog, are presented together. The different terminal ligands of **7, 8**, and **9** shift the energy of the MLCT and the π–π* transition of the bridging ligand. These shifts in the spectra are discussed in the context of density functional theory (DFT). A model is proposed suggesting that low-lying orbitals of the bridging ligand accept electron density from the metal center which can facilitate electron transfer to nanoparticles like single walled carbon nanotubes and colloidal gold.

1. Introduction

Understanding directed self-assembly of supramolecular systems is critical to the development of nanoscale devices. Dendrimer chemistry continues to provide both building blocks and scaffolds for supramolecular and nanodevice engineering [1–4]. Metallodendrimers are of broad interest because of their potential use in light harvesting, sensing, signal amplification, and electron-transfer reagents in water splitting applications [4–6]. Optically and electrochemically active ruthenium metallodendrimers possess several properties which enable their versatility in supramolecular systems. By changing the morphology and the local charge density of the ruthenium complexes, we have studied how these mononuclear and decanuclear metallodendrimers (decamers) [7] interact with and coordinate to single walled carbon nanotubes (SWNT) [2,3,8]. Towards this end, novel dinuclear ruthenium coordination complexes (dimers) have been synthesized. The results presented below will enable further studies of the optoelectronic properties of ruthenium coordination compounds and their interactions with nanoparticles. Specifically these new compounds will help us discriminate between the supramolecular interactions due to molecular morphology and the interactions due to the electron density distributions and net molecular charge on the compounds.

We have synthesized two structurally similar ruthenium dimers with differing electrostatic charges. Both complexes are composed of two ruthenium monomer units bridged by the aromatic tetrapyrido[3,2-α:2′,3′-c:3″,2″-h:2″,3″-j]phenazine (tpphz) ligand. Coordinating various ligands to the ruthenium monomer precursors allows us to specify the charge state of the resulting dimer as either +2, +3, or +4. The new ruthenium complexes produced through this method are $[Cl(terpy)Ru(tpphz)Ru(terpy)Cl](PF_6)_2$ **(7)** and $[(phen)_2Ru(tpphz)Ru(terpy)Cl](PF_6)_3$ **(8)**. These complexes are similar in structure to the +4 complex $[(phen)_2Ru(tpphz)Ru$-$(phen)_2](PF_6)_4$ **(9)**, previously reported by MacDonnell et al. [9]. In addition to the ruthenium dimer synthesis we report a mixed solvent synthesis method for their precursor, $Ru(DMSO)_4Cl_2$ **(3)**. By using a mixed solvent, product readily precipitates from solution as it is formed, simplifying collection while maintaining high purity with yields of approximately 90% [10,11].

By comparing our new compounds to **9**, we were able to investigate how different electrostatic charges affect the optical properties of structurally similar ruthenium complexes. Our results show that the MLCT absorption is more red-shifted as the charge state is lowered. DFT level calculations of the highest occupied molecular orbital (HOMO) and the lowest unoccupied molecular orbital (LUMO) of the +2, +3, and +4 dimers suggest that electron density

* Corresponding author. Tel.: +1 704 687 8289; fax: +1 704 687 3151.
E-mail address: jcpoler@uncc.edu (J.C. Poler).

0277-5387/$ - see front matter © 2010 Elsevier Ltd. All rights reserved.
doi:10.1016/j.poly.2010.06.012

shifts from the ruthenium centers to the tpphz bridge during the MLCT transition. The dimensions and molecular rigidity of **7, 8**, and **9** are configured to interact effectively with nanoparticles. Catalytic metal nanoparticles, quantum dots and rods, and nanotubes are targets for non-covalent, site specific functionalization and sensitization by these coordination compounds. Because we can effectively manipulate the optoelectronic properties of these ruthenium complexes and the overall charge-state while maintaining their rigid structure, we aim to use complexes like **7, 8**, and **9** as potential building blocks and integral components in the design of supramolecular nanoscale systems.

2. Experimental

2.1. Materials and methods

1,10-Phenanthroline (phen), $RuCl_3{\cdot}3H_2O$, dimethyl sulfoxide (DMSO), 2,2′;6′,2″-terpyridine (terpy), hydrazine hydrate, and palladium/carbon catalyst were purchased from Sigma–Aldrich or Alfa and were used without further processing or purification unless otherwise noted. 1,10-Phenanthroline-5,6-dione (phendione) [12,13], 1,10-phenanthroline-5,6-diamine (phendiamine), and tpphz **(6)** [14] were prepared *via* literature procedures with any variations noted herein. *cis*-$RuCl_2(phen)_2$ **(1)** [15] was prepared *via* literature procedures substituting phen for bipyridine (bipy). $[Ru(phen)_2phendione](PF_6)_2$ **(2)** [13] and $RuCl_2(DMSO)_4$ **(3)** [10,11,16,17] were prepared through a slight adaptation of literature procedures. $RuCl_2$(terpy)DMSO **(5)** [18] was prepared with slight variations to literature procedures with changes noted below. $[(phen)_2Ru(tpphz)Ru(phen)_2](PF_6)_4$ **(9)** was prepared following literature methods [9,14]. All solvents were analytical grade and dried on molecular sieves when applicable.

C, H, and N elemental analysis was performed by Atlantic Microlab, Inc. ^1H and ^{13}C NMR spectra of **7**, **8**, and **9** in DMSO-d_6 were obtained at room temperature on a JEOL 500 MHz Fourier Transform (FT) spectrometer unless otherwise noted. Chemical shifts are reported in parts per million (ppm) using TMS as an internal reference for ^1H and ^{13}C. Assignment of ^1H NMR peaks for **7** and **8** were accomplished by high resolution phase sensitive COSY 2D ^1H NMR. ESI mass spectrometry was performed in positive ion mode on a Mariner Biospectrometry Workstation in acetonitrile. All *m*/*z* are reported for the most abundant isotope and $[Ru_2{-}XPF_6^-]$ represents the dinuclear species without X of its associated PF_6^- counterions. Electronic absorption spectra were recorded on a Varian Cary 5000 spectrometer in dimethylformamide (DMF) or acetonitrile (MeCN). Infrared (IR) spectra were obtained on a Perkin–Elmer Spectrum One FT-IR with a universal diamond attenuated total reflectance top plate. Melting/degradation points (MP_{deg}) of **7** and **8** were measured on a Mettler-Toledo Thermogravimetric Analysis TGA/SDTA 851e under $N_{2(g)}$ atmosphere. Photodegradation studies were done in air saturated DMF under a 5 mW illumination of a 450 (±5) nm source for 12 h. Limiting molar conductivity (Λ°_m, S cm^2 mol^{-1}) in DMF was determined from Kohlrausch's law using conductivity data from an Accumet AR20 calibrated with a $KCl_{(aq)}$ standard.

2.2. Synthesis of ruthenium coordination complexes

2.2.1. *cis*-$RuCl_2(phen)_2$ **(1)**

LiCl and $RuCl_3{\cdot}3H_2O$ were dried under vacuum at 125 °C for 15 h. A mixture of LiCl (8.89 g, 210 mmol), $RuCl_3$ (5.33 g, 25.0 mmol), phen (7.11 g, 40.0 mmol), and DMF (40 mL) was stirred and refluxed for 15 h. The purple/black solution was cooled to room temperature (RT) and then rinsed from the reaction flask and diluted with acetone (500 mL). This solution was then kept at 0 °C for 12–15 h. The resulting purple/black solid precipitate was collected by filtration. The product was washed with acetone (50 mL, 2×) and then several times with ice cold water (30 mL, 3×), yielding a dark purple solid. This compound is used best without further purification due to degradation during recrystallization. Yield: 6.85 g, 65%; UV–Vis (DMF) λ_{MLCT} 552 nm (ε = 3400 M^{-1} cm^{-1}).

2.2.2. $[Ru(phen)_2phendione](PF_6)_2$ **(2)**

A mixture of absolute ethanol (50 mL) degassed with $Ar_{(g)}$, complex **1** (0.408 g, 0.80 mmol), and phendione (0.210 g, 1.0 mmol) was stirred and refluxed under an inert atmosphere of $Ar_{(g)}$ for 24 h. After the mixture was cooled to RT, a saturated $KPF_{6(aq)}$ solution was added dropwise to precipitate the brown product. The solution was kept at 4 °C for 12–15 h and the brown solid was collected by filtration. The solid was washed with cold ethanol (95%, 20 mL, 3×), then with cold absolute ethanol (20 mL, 2×), and finally with diethyl ether (20 mL, 2×). The yellow brown solid was air dried. Yield: 0.490 g, 66%; UV–Vis (MeCN) λ_{MLCT} 430 nm (ε = 14,000 M^{-1} cm^{-1}).

2.2.3. *cis,fac*-$RuCl_2(DMSO\text{-}S)_3(DMSO\text{-}O)$ **(3)**

DMSO (10 mL) was degassed with $Ar_{(g)}$ for 20 min. $RuCl_3{\cdot}3H_2O$ (3.247 g, 12.0 mmol) was added to the DMSO and stirred under $Ar_{(g)}$ until dissolved. Isopropanol (35 mL) was then added, and the light orange solution was heated at 85 °C under an inert atmosphere of $Ar_{(g)}$ for 30 h. During heating, the product readily precipitated from solution. After the reaction was cooled to RT, the bright yellow precipitate was broken up with a glass rod and collected by vacuum filtration, washed liberally with dry acetone, rinsed liberally with toluene, and finally dried on the filter. Yield: 5.240 g, 87%; UV–Vis (MeCN) λ_{max} 356 nm (ε = 380 M^{-1} cm^{-1}). Selected FT-IR absorptions, cm^{-1}: ν(DMSO-S) 1083.1 (s), ν(DMSO-O) 923.4 (s).

2.2.4. $[Ru(phen)_2tpphz](PF_6)_2$ **(4)**

A mixture of **2** (0.200 g, 0.20 mmol) in acetonitrile (10 mL) was stirred and brought to a boil. A separate volume of methanol (35 mL) was heated to a boil then phendiamine (0.051 g, 0.20 mmol) was dissolved into the hot methanol. The hot phendiamine solution was added to the boiling acetonitrile solution containing **2** and brought to reflux while stirring under $Ar_{(g)}$ for 5 h. The reaction was cooled to RT, and then saturated $KPF_{6(aq)}$ was added dropwise until the brown precipitate stopped forming. The precipitate was collected by vacuum filtration and the solid washed with ice cold water (20 mL, 2×), cold ethanol (95%, 20 mL, 2×), and finally with diethyl ether (20 mL, 2×). The brown solid was dried on the filter. Yield: 0.168 g, 71%; UV–Vis (MeCN) $\lambda_{tpphz\ \pi\text{–}\pi^*}$ 385 nm (ε = 28,000 M^{-1} cm^{-1}), λ_{MLCT} 455 nm (ε = 19,700 M^{-1} cm^{-1}). ESI-MS: $[Ru{-}2PF_6^-]^{2+}$ *m*/*z* = 423.1, $[Ru{-}1PF_6^-]^+$ *m*/*z* = 192.2. ^1H NMR: 300 MHz (CD_3CN) δ (ppm): 9.80 (d, *J* = 8.25 Hz, 2H), 9.71 (d, *J* = 7.32 Hz, 2H), 9.01 (d, 2H), 8.65 (d, *J* = 2.76 Hz, 2H), 8.62 (d, *J* = 2.76 Hz, 2H), 8.40 (d, *J* = 4.77 Hz, 2H), 8.23 (s, 4H), 8.19 (d, *J* = 5.52 Hz, 2H), 8.06 (d, *J* = 5.13 Hz, 2H), 7.92 (dd, *J* = 8.43, 2H), 7.81 (dd, *J* = 8.04, 2H), 7.68 (m, 4H).

2.2.5. $RuCl_2$(terpy)DMSO (**5**)

A mixture of ethanol (95%, 20 mL) and methanol (6 mL) was slowly stirred as **3** (1.263 g, 2.20 mmol) was added. The mixture was stirred and refluxed under an inert $Ar_{(g)}$ atmosphere for 15 min. A separate mixture of ethanol (95%, 10 mL) and terpy (0.604 g, 2.6 mmol) was prepared and slowly transferred under $Ar_{(g)}$ to the refluxing solution of **3**. The resulting brown mixture was refluxed and stirred under $Ar_{(g)}$ for another 8.5 h. The brown precipitate was collected by vacuum filtration. The solid was washed with cold water (20 mL, 3×), and then cold ethanol (95%)

until the filtrate was clear and colorless. The brown product was vacuum dried at 90 °C. Yield: 0.916 g, 88%; UV–Vis (MeCN) λ_{MLCT} 513 nm (ε = 3000 M^{-1} cm^{-1}).

2.2.6. [Cl(terpy)Ru(tpphz)Ru(terpy)Cl](PF$_6$)$_2$·5H$_2$O (**7**)

A mixture 0.166 g (0.40 mmol) of **6** and 0.415 g (0.90 mmol) of complex **5** were added to a mixed solvent solution of ethanol (95%, 15 mL) and water (15 mL). The resulting solution was stirred and refluxed for 24 h. After the reaction was cooled to RT, the dark purple mixture was brought to dryness under vacuum, and then the residue was dissolved in a minimal amount of water (~30 mL). The dark purple solution was added dropwise to a saturated $KPF_{6(aq)}$ solution to yield a precipitate. The purple solid was collected by vacuum filtration, and then washed with water until the filtrate was clear and colorless. The solid was dried under vacuum at 90 °C. Yield: 0.468 g, 77%; UV–Vis (DMF) $\lambda_{tpphz\ \pi-\pi^*}$ 375 nm (ε = 33,000 M^{-1} cm^{-1}), λ_{MLCT} 518 nm (ε = 28,000 M^{-1} cm^{-1}). Melting point of degradation (MP_{deg}): 356 °C. *Anal.* Calc. for $C_{54}H_{34}N_{12}$–$Ru_2P_2F_{12}$·5H_2O: C, 43.12; H, 2.95; N, 11.18. Found: C, 43.13; H, 2.60; N, 10.87%. Limiting molar conductivity, $\Lambda°_m$: 230 S cm^2 mol^{-1}. ESI-MS: $[Ru_2-2PF_6^-]^{2+}$ m/z = 562.1, $[Ru_2-1PF_6^-]^+$ m/z = 1269.3. ^{1}H NMR (DMSO-d_6) δ (ppm): 10.57 (d, J = 5.15 Hz, tpphz), 10.53 (d, J = 4.60 Hz, tpphz), 10.38 (d, J = 8.30 Hz, tpphz), 10.21 (d, J = 5.70 Hz, tpphz), 10.18 (d, J = 9.15 Hz, tpphz), 9.82 (d, J = 8.05 Hz, tpphz), 9.62 (d, 8.00 Hz, tpphz), 8.89 (d, J = 8.05 Hz, terpy 2H), 8.84 (d, J = 8 Hz, tpphz), 8.37–8.24 (m, tpphz and terpy 4H), 8.37–8.24 (m, tpphz and terpy 4H), 8.04–7.90 (m, tpphz and terpy 4H), 7.73 (d, J = 6.30 Hz, terpy 4H), 7.77–7.62 (m, tpphz), 7.44 (apparent dd, J = 6.30 Hz, tpphz), 7.32–7.27 (m, tpphz and terpy 4H); ^{13}C NMR (DMSO) δ 158.24, 157.51, 152.48, 151.60, 149.54, 137.11, 127.21, 123.65, 122.73.

2.2.7. [(phen)$_2$Ru(tpphz)Ru(terpy)Cl](PF$_6$)$_3$·2H$_2$O ***(8)***

A mixture of **4** (0.105 g, 0.10 mmol), **5** (0.046 g, 0.10 mmol), and DMF (15 mL) were stirred and refluxed under $Ar_{(g)}$ for 23 h. The reaction was cooled to RT, and then saturated $KPF_{6(aq)}$ was added

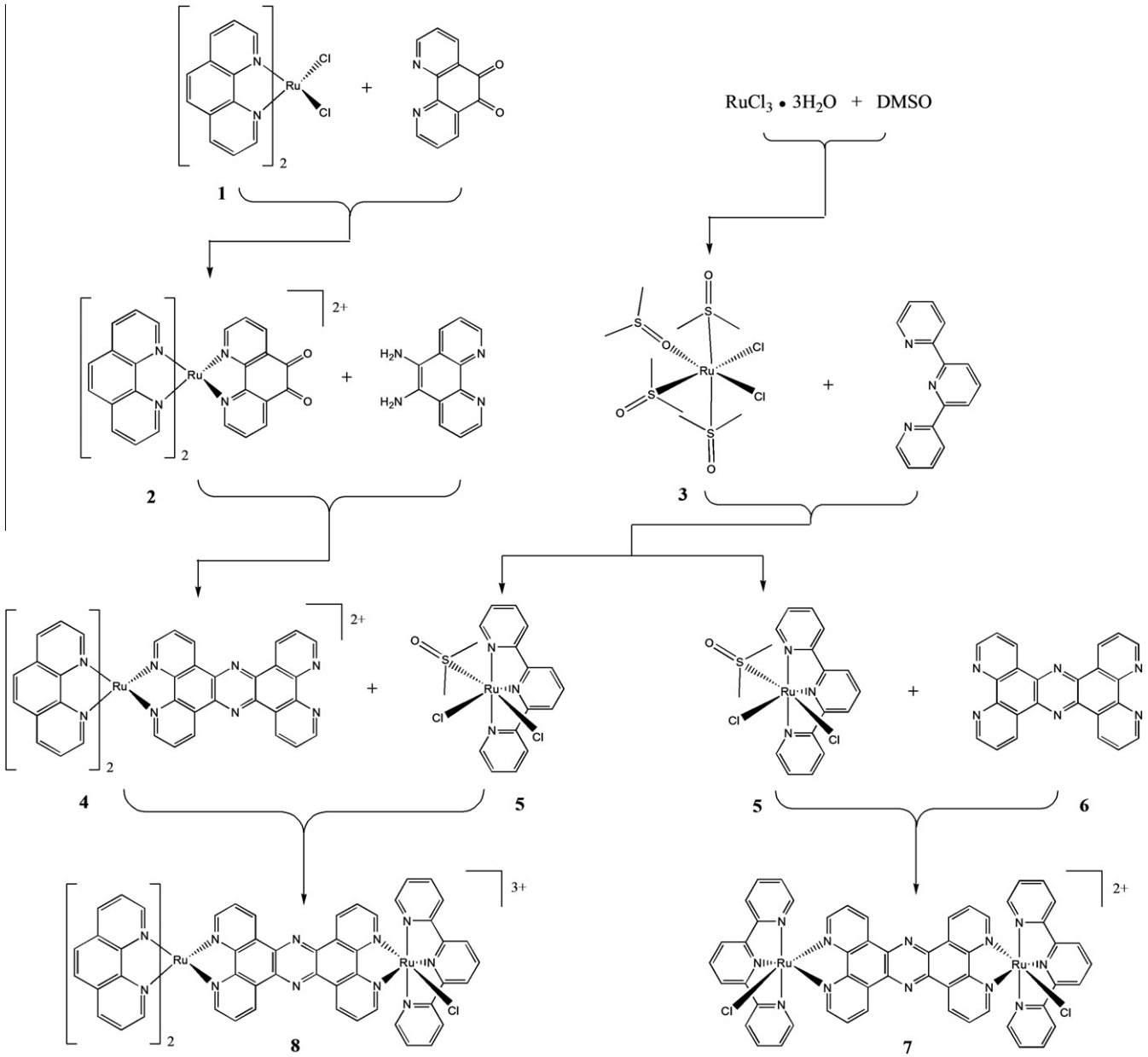

Scheme 1. Reaction sequence for the synthesis of +2 Ru dimer (**7**) and +3 Ru dimer **(8)**.

dropwise, producing a reddish precipitate. The mixture was then held at 4 °C for 12 h. The dark orange-red solid was collected by vacuum filtration, washed with cold water (20 mL, 2×), and then cold ethanol (95%, 20 mL, 2×), and finally with diethyl ether (20 mL, 2×) and dried under vacuum at 90 °C for 12 h. Yield: 0.087 g, 52%; UV–Vis (DMF) $\lambda_{tpphz\ \pi-\pi^*}$ 375 nm (ε = 35,000 $M^{-1}\,cm^{-1}$), λ_{MLCT} 453 nm (ε = 26,000 $M^{-1}\,cm^{-1}$). MP_{deg}: 370 °C. *Anal.* Calc. for $C_{63}H_{39}N_{13}$–$Ru_2P_3F_{18}{\cdot}2H_2O$: C, 44.86; H, 2.57; N, 10.80. Found: C, 44.47; H, 2.46; N, 10.87%. Limiting molar conductivity, Λ°_m: 310 S cm^2 mol^{-1}. ESI-MS: $[Ru_2{-}3PF_6^-]^{3+}$ m/z = 405.4, $[Ru_2{-}2PF_6^-]^{2+}$ m/z = 680.5, $[Ru_2{-}1PF_6^-]^{+}$ m/z = 1506.1. ^{1}H NMR (DMSO-d_6) δ (ppm): 10.54 (d, J = 5.20 Hz, 1H), 10.26 (d, J = 8.05 Hz, 1H), 10.18 (d, J = 7.45 Hz, 1H), 9.97 (d, J = 8.00, 1H), 9.70 (d, J = 8.00 Hz, 1H), 8.91 (d, J = 8.05 Hz, 1H), 8.81 (app. t, J = 8.00 Hz, 4H), 8.76 (d, J = 8.00 Hz, 2H), 8.72 (dd, 8 Hz, 1H), 8.43 (d, J = 6.90 Hz, 4H), 8.34–8.26 (m, 4H), 8.12–8.06 (m, 5H), 8.01–7.95 (m, 3H), 7.85–7.77 (m, 5H), 7.71 (app. d, 2H), 7.30 (dd, 12.6 Hz, 3H); ^{13}C NMR (DMSO-d_6) δ 158.26, 157.51, 154.42, 153.17, 152.50, 152.49, 151.71, 150.33, 149.64, 147.05, 139.69, 137.16, 136.92, 130.40, 129.40, 128.63, 127.99, 127.21, 126.31, 123.68, 122.77.

3. Results and discussion

3.1. Synthesis of **3**

Addition of $RuCl_3{\cdot}3H_2O$ in DMSO to give **3** can yield either *cis* or *trans* isomers [16]. X-ray crystallography has previously shown the *cis* product coordinates one of the DMSO ligands through the oxygen and the other three through the sulfur while the *trans* product coordinates DMSO exclusively through sulfur [17]. The kinetically stable isomer, *trans*-$RuCl_2$(DMSO-S)$_4$, should be the most likely product at low temperatures (<100 °C) [19], whereas the thermodynamically stable isomer, *cis,fac*-$RuCl_2$(DMSO-S)$_3$(DMSO-O), should be the primary product of $RuCl_3$ in hot (120–150 °C) DMSO [11,17]. The synthesis procedure described above was performed at low temperature (85 °C) in mixed solvent. Under low temperature, mixed solvent conditions, we observe the synthesis of pure *cis,fac*-$RuCl_2$(DMSO-S)$_3$(DMSO-O). Using FT-IR spectroscopy, the as-produced product was analyzed to determine the orientation of the coordinated DMSO from our mixed solvent procedure. The S=O stretching frequency of uncoordinated DMSO is approximately 1055 cm^{-1} [20]. This transition is not found in our IR therefore we do not observe any uncoordinated DMSO in this sample. The stretching frequency of Ru–S-bonded DMSO is reported to resonate at 1080 cm^{-1}. While the Ru–O-bonded DMSO stretching frequency is reported to appear between 890 and 950 cm^{-1} [20,21], we experimentally detected stretching frequencies at 923.4 cm^{-1} and 1083.1 cm^{-1} from our as-produced sample suggesting the *cis* product. Following procedures reported by Alessio et al. [16] we converted samples of $RuCl_2(DMSO)_4$ to the pure *cis* and pure *trans* isoforms. IR spectra of the pure samples were overlaid with that of the as-produced sample and compared (Supplementary Fig. S1). The spectra of the pure *cis,fac*-$RuCl_2$(DMSO-S)$_3$(DMSO-O) is identical to that of our as-produced product. The spectra of the pure *trans*-$RuCl_2$(DMSO-S)$_4$ not only lacks the stretching frequency of Ru–O-bonded DMSO, the frequency of Ru–S-bonded DMSO is at a lower energy, ν1076.7 cm^{-1}, versus ν1083.1 cm^{-1} in the *cis* spectra. The lower vibrational transition energy is likely caused by the decrease of ruthenium electron donation due to the additional S-bonded DMSO competition [20].

Exclusive production of the thermodynamically favored *cis* isoform even at low reaction temperatures can be explained by the solubility of the different isomers in the mixed solvent environment. To produce $RuCl_2(DMSO)_4$ it is common to use DMSO both as a reactant and the primary solvent. In these cases the *cis* product is very soluble in DMSO while the *trans* product can precipitate as the reaction mixture cools [16,17,20,21]. Temperature tends to be the isoform determining factor during these reactions. During our synthesis procedure we chose to use DMSO as a reactant in slight excess and use isopropanol (IPA) as the primary solvent. Isopropanol was selected as a solvent due to the limited solubility of $RuCl_2(DMSO)_4$ which had the intended consequence of precipitating product as it was formed, simplifying the collection of product. The solubility of *cis* isoform in IPA is 0.6 mg/mL while the solubility of the *trans* isoform is 5.0 mg/mL.

3.2. Synthesis and stability of **7** and **8**

Reaction Scheme 1 illustrates the two synthetic routes through which we manipulated the final charge state and optical properties of **7** and **8**. The phen derivatives, 1,10-phenanthroline-5,6-dione [12,13], 1,10-phenanthroline-5,6-diamine [14], and tpphz [14] were produced *via* previously reported synthetic procedures. Complex **7** was synthesized from a ligand exchange reaction of two molar equivalents of **5** and one molar equivalent of **6**. Complex **8** was synthesized from a ligand exchange reaction between **5** and the PF_6 salt of **4**. Following synthesis, compounds **7** and **8** were characterized by EA, UV–Vis, SDTA, ESI-MS, ^{1}H NMR, and ^{13}C NMR. ESI-MS was essential to identifying and characterizing the compounds. There are seven ruthenium isotopes with large enough natural abundances to be measured in ESI-MS. The signature of a mononuclear complex is easily distinguished (7 isotope peaks) from the isotope patter of a dinuclear species (13 easily identified peaks for one complex). There was no observable monomer in the ESI-MS of any of the dimers reported here. The dimers show excellent stability in solution. Each dimer has a unique mass to charge (m/z) pattern. The calculated isotope patterns of **7**, **8**, and **9** accurately match the measured mass spectrum (Supplementary Fig. S2). The difference in m/z within the isotope pattern allows us to determine the absolute charge on the species. When the resulting isotope peaks are separated by 1.0 m/z unit the overall electrostatic charge on the complex is +1. Correspondingly, the separation is 0.50 m/z units for +2 and 0.33 m/z units for +3, and 0.25 m/z units for a +4 charge.

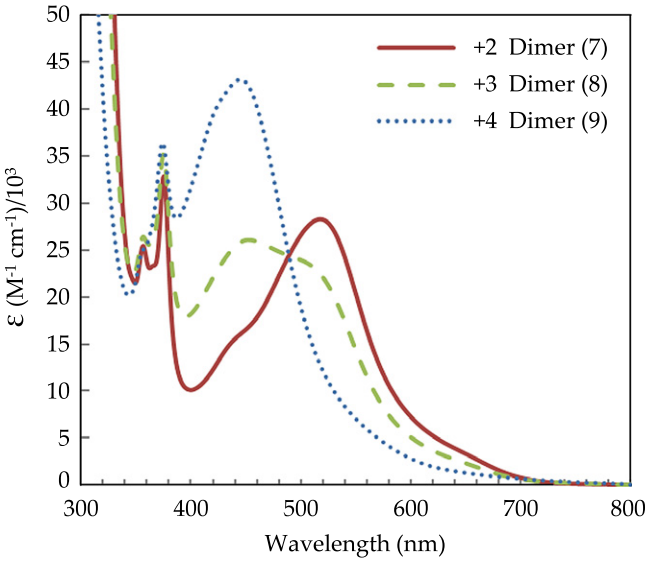

Fig. 1. UV–Vis absorption spectra of complexes **7**, **8**, and **9**. Complex **7** λ_{MLCT} 518 nm (ε = 28,000 $M^{-1}\,cm^{-1}$), complex **8** λ_{MLCT} 453 nm (ε = 26,000 $M^{-1}\,cm^{-1}$), and complex **9** λ_{MLCT} 444 nm (ε = 41,000 $M^{-1}\,cm^{-1}$).

Thermal stability of the ruthenium coordination complexes **7, 8**, and **9** were measured using scanning differential thermal analysis, SDTA (Supplementary Fig. S3). The dimers were thermally stable under $N_{2(g)}$ up to 356 °C. Complex **7** began decomposing at 356 °C, noted as the melting point onset temperature of degradation (MP_{deg}) for the PF_6 salt. Complexes **8** and **9** followed suit, beginning decomposition at 370 °C and 380 °C, respectively. Photodegradation of **7**, **8**, and **9** evaluated with UV–Vis showed no measurable decomposition after 12 h of 5 mW/cm^2 of 450 (±5) nm illumination. A series of ^{1}H NMR spectra as a function of time showed that the ruthenium coordination complexes are air stable. Uncoordinated phendiamine was prone to degradation. We use the phendiamine immediately after it was prepared to synthesize **6**. The other uncoordinated polypyridine ligands such as phen-5,6-dione, 5-nitro-phen and terpy are air and light stable.

3.3. ^{1}H NMR of *7*, *8*, and *9*

On the basis of previous reports [7,14,22,23] and the spectra of **9**, used in conjunction with high resolution phase sensitive COSY 2D spectroscopy, the proton signals of **7** and **8** were assigned. The large distance between the ancillary ligands of **9** and the tpphz bridge make it so the ^{1}H NMR spectra of all eight magnetically inequivalent protons belonging to the same ancillary phens overlap identically [22]. The magnetic patterns of **7** and **8** are complex (Supplementary Fig. S4). The protons of the terpy ligands are easily distinguished. However, the asymmetric heteroleptic arrangement of **8** as well as the presence of *syn* and *anti* forms of **7** produce anisotropic magnetic effects on the pyridine cycle of tpphz. The magnetic inequivalence of the tpphz protons presents 12 distinct proton signals in the spectra of **8**. For **7**, there are two isomers. The chloride ligand on either ruthenium core can be in *syn* and *anti* arrangements. These isomers are likely formed in equal amounts. The presence of the isomers in solution can be observed by the shielding effect of the chloride ligand on the proximal H2 protons of tpphz. The shielding reduces the *J* coupling to approximately 5 Hz between the H2 and H3 protons of the tpphz. Complex **8** has two diastereomers which produce similar chloride shielded H2 signals at 10.54 ppm. The two isomers of **7** will have slight differences in H2 resonances and produce three shielded signals at

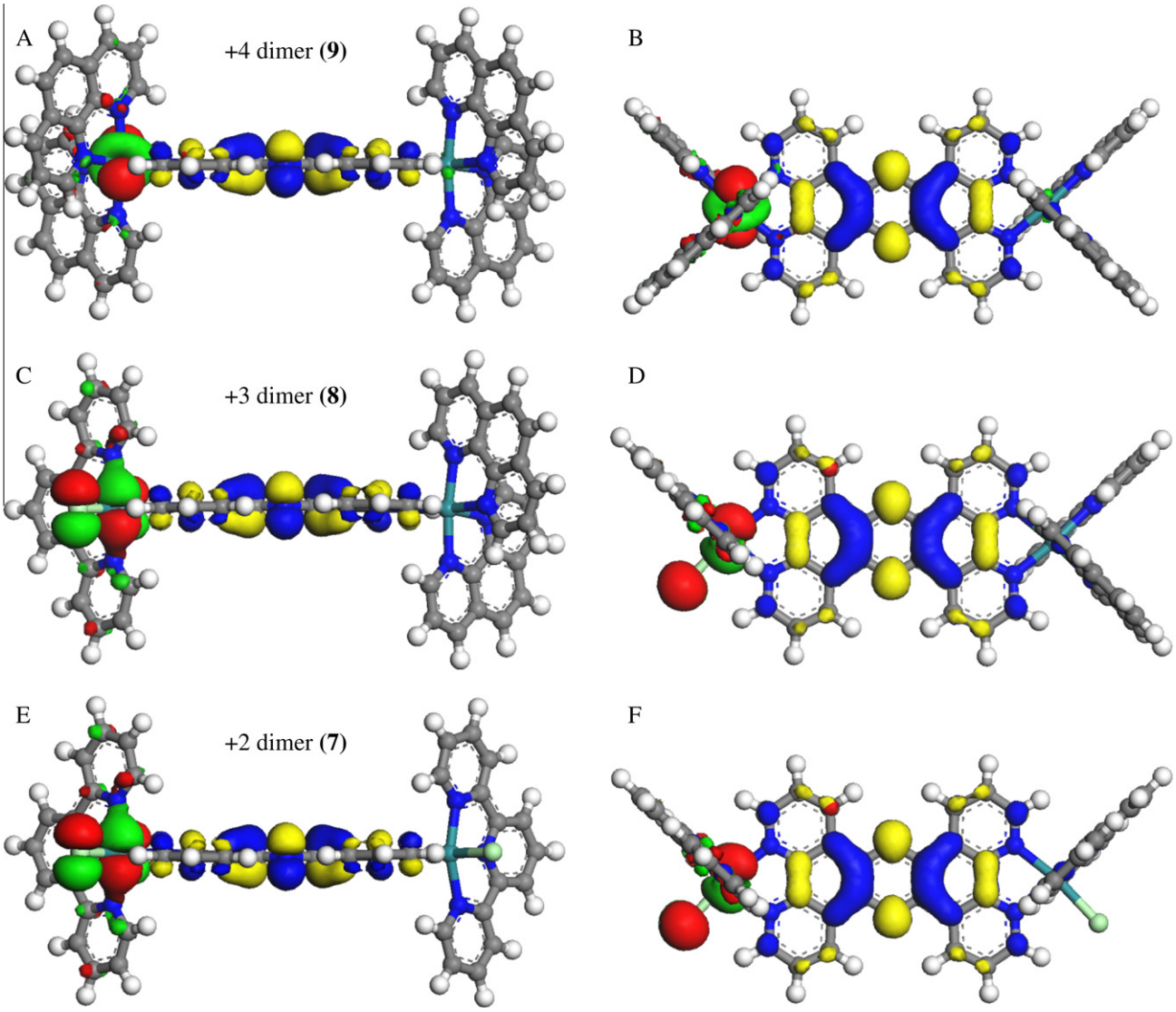

Fig. 2. Frontier molecular orbitals for dinuclear Ru complexes. (A, C, E) illustrate the +4, +3, and +2 dimers, respectively looking along the tpphz edge, and (B, D, F) illustrate +4, +3, and +2 dimers, respectively looking perpendicular to the tpphz ligand. The HOMO is depicted on the Ru center and colored green–red; the LUMO is located across the tpphz bridge and colored blue–yellow. Notice the LUMO is similar across species whereas the HOMO at the Ru centers varies depending on the presence of chloride ligand. The only significant difference between the enhanced d_z^2 character on the Ru center of the +4 dimer (A, B) as compared to the orbital on the chloride on the +2 dimer (E, F). (For interpretation of the references to colour in this figure legend, the reader is referred to the web version of this article.)

10.57, 10.53, and 10.21 ppm. COSY 2D NMR aided the assignment of the tpphz protons. To distinguish between the protons, the deshielding effects of the ancillary ligands were considered. Those tpphz protons opposite phen ligands would be furthest downfield, followed by those opposite terpy and then chloride [24]. For simplicity, proton peaks presented for **7** are integrated only for the terpy signals. These observations are in complete agreement with the data reported for the mononuclear $[Ru(L)_2tpphz]^{2+}$ complexes [L = phen or bipy] [22,23].

3.4. Electronic spectral studies

The absorption spectra of **7**, **8**, and **9** in DMF are shown in Fig. 1. As observed for uncoordinated polypyridine ligands and mononuclear ruthenium complexes the ruthenium dimer complexes retain similar spectral features. The absorption spectra for compounds **7, 8**, and **9** show an absorption at approximately 375 nm with a higher energy shoulder for **9** which evolves into another peak for **7** and **8**. These two bands correspond to the (tpphz)n–π^* and (tpphz)π–π^* transitions [14]. This π–π^* transition is red-shifted compared to the corresponding λ_{max} of 365 nm for uncoordinated tpphz due to the back-donation from the ruthenium (Supplementary Fig. S5).

Each ruthenium dimer displays a strong and characteristic MLCT band at 400–600 nm. For **7** the MLCT bands are attributed to the overlap of Ru → tpphz(π^*) and Ru → terpy(π^*). The MLCT bands of **8** appear more broad which is attributed to the overlap of Ru → phen(π^*) and Ru → tpphz(π^*) from one half of the dimer combining with the overlap of Ru → tpphz(π^*) and Ru → terpy(π^*) from the other half. For comparison the absorption spectra of **9** in Fig. 1 and the spectra of polypyridine coordinated ruthenium monomers (Supplementary Fig. S6) are included. The MLCT bands of **9** have been reported and assigned to the corresponding transitions, Ru → phen(π^*) and Ru → tpphz(π^*), which correlate well with our observations [7,14,22,25]. A red-shift from **9** of the MLCT bands for **7** and **8** is observed, with decreasing energy relative to their formal charge. The electron density over ruthenium, the location of the HOMO (*vide infra*), is increased due to the coordination of chloride ligands and also by the smaller back-donation from ruthenium to terpy versus ruthenium to two phens. The increased electron density narrows the energy difference between the HOMO and LUMO of the molecule, shifting the MLCT transition to the red [14].

3.5. Molecular modeling

DFT calculations were completed with Materials Studio 4.4 (Accelrys) using a gradient corrected Becke, Lee, Yang, and Parr functional. All core electrons were treated fully and with relativistic effects. A self consistent field tolerance of 10^{-6} Ha and geometry optimization tolerance of 10^{-5} Ha were imposed with a maximum atom displacement of 0.005 Å (or a maximum force gradient of 0.002 Ha/Å). All optimizations were treated with a conductor-like screening model with a dielectric constant of 36.7 to simulate DMF, the solvent used for our electronic spectral studies. Frontier molecular orbitals for the three dimers are shown (Fig. 2). Although **7** and **8** have electron donating chlorides on at least one of their ruthenium centers, the shape and distribution of the LUMO across the tpphz bridge is almost identical between compounds **7, 8**, and **9**. Interestingly, the most prominent difference between each compound was observed in the HOMO. Orbitals on the ruthenium centers of **9**, the +4 complex, had very strong d_z^2 character. The HOMO through HOMO-5 orbitals of **9** were similar on the two metal centers and nearly degenerate ($<7 \times 10^{-4}$ Ha). The HOMO through HOMO-5 orbitals of **7** were also similar and nearly degenerate ($<7 \times 10^{-4}$ Ha). These molecular orbitals overlap both the metal center and the chloride ligand. In contrast, the HOMO through HOMO-5 orbitals on **8** all resided on the metal center with the chloride ligand. We have also completed excited state calculations using configuration interaction singles with the semi-empirical Zerner's Independent Neglect of Differential Overlap (ZINDO) Hamiltonian. The transition energies, determined using this model, are consistent with our observation that the MLCT transition is red-shifted as the charge state is lowered. These computational models are consistent with our spectrometric observations.

4. Conclusions

In summary, in this work we have presented the synthesis of two new heteroleptic dinuclear ruthenium(II) coordination complexes, $[Cl(terpy)Ru(tpphz)Ru(terpy)Cl](PF_6)_2$ **(7)** and $[(phen)_2Ru(tpphz)Ru(terpy)Cl](PF_6)_3$ **(8)**. It has been demonstrated that the two compounds are stable and have been produced in good yield. The optical absorption of these complexes, specifically the MLCT transitions have been shown to be influenced by the electron withdrawing nature of ligands opposite the tpphz bridging ligand. Both complexes exhibit characteristic electronic absorption spectra that correlate well with the morphologically similar +4 dimer **(9)** and with the calculated HOMO and LUMO of both complexes. It is important to note that regardless of the varying terminal ligands or the resulting charge state of the dimer, the calculated molecular orbitals show that the LUMO maintains a similar shape on all three complexes while predominantly residing on the bridging ligand between the two ruthenium centers. Our ZINDO calculated transition energies lack accuracy, but are consistent with our observed trends in the shifting MLCT bands of **7, 8**, and **9**. Time dependent DFT studies are required to further analyze the differences in these spectra. Presently, our data supports previous work suggesting that ruthenium complexes bridged by tpphz could interact with nanoscale materials through the extension of that complex's electron density [1–3]. This phenomena can be stimulated by optical excitation of a MLCT band [3] which we have shown resides solely on the bridging ligand and in the nanoscale pocket formed by the rigid structure.

The complexes synthesized herein are new members of a nascent family of rigid ruthenium complexes that have optical properties that could be useful for controlling nanoparticle interactions as well as being utilized in charge transfer applications. Using the synthetic strategies described above we are able to shift the MLCT band to longer wavelengths enabling a more efficient overlap with the solar spectrum, which implies more utility for involvement in photovoltaic and photocatalytic applications. Preliminary results show strong interactions with nanoparticles such as carbon nanotubes and metal nanoparticles and show great potential for becoming building blocks and scaffold for technologically viable supramolecular structures with specified shape and charge [1,3,8]. The key to this goal is a better understanding of how morphology and charge state of supramolecular systems affects their optoelectronic properties. Further study and synthesis of photoactive ruthenium coordination complexes as well as study of nanostructures that integrate rigid coordination complexes will hopefully contribute to this goal.

Acknowledgement

Acknowledgement is made to the Donors of the American Chemical Society Petroleum Research Fund for partial support of this research. Financial support to JRA through the Nanoscale Science Ph.D. program and the Center for Optoelectronics and Optical Communications at UNC Charlotte is appreciated. Financial support to SK through a Thomas Walsh Fellowship and UNC Charlotte

is appreciated. The authors would also like to thank Dr. Schmedake, Dr. Cliff Carlin, Dr. Jon Merkert, Dr. Michael Murphy, and Dr. John Pickett for instrumental assistance and discussion.

Appendix A. Supplementary data

Supplementary data associated with this article can be found, in the online version, at doi:10.1016/j.poly.2010.06.012.

References

[1] H. Chaturvedi, A.N. Giordano, M.J. Kim, F.M. MacDonnell, S.S. Subaran, J.C. Poler, J. Phys. Chem. C 113 (2009) 11254.
[2] H. Chaturvedi, J.C. Poler, J. Phys. Chem. B 110 (2006) 22387.
[3] H. Chaturvedi, J.C. Poler, Appl. Phys. Lett. 90 (2007) 3.
[4] V. Balzani, G. Bergamini, P. Ceroni, Coord. Chem. Rev. 252 (2008) 2456.
[5] S.M. Arachchige, J.R. Brown, E. Chang, A. Jain, D.F. Zigler, K. Rangan, K.J. Brewer, Inorg. Chem. 48 (2009) 1989.
[6] V. Balzani, S. Campagna, G. Denti, A. Juris, S. Serroni, M. Venturi, Acc. Chem. Res. 31 (1998) 26.
[7] F.M. MacDonnell, M.J. Kim, S. Bodige, Coord. Chem. Rev. 185–186 (1999) 535.
[8] A.N. Giordano, H. Chaturvedi, J.C. Poler, J. Phys. Chem. C 111 (2007) 11583.
[9] F.M. MacDonnell, S. Bodige, Inorg. Chem. 35 (1996) 5758.
[10] B.R. James, E. Ochiai, G.I. Rempel, J. Inorg. Nucl. Chem. 7 (1971) 781.
[11] I.P. Evans, A. Spencer, G. Wilkinso, J. Chem. Soc.-Dalton Trans. (1973) 204.
[12] J.E. Dickeson, L.A. Summers, Aust. J. Chem. 23 (1970) 1023.
[13] C. Hiort, P. Lincoln, B. Norden, J. Am. Chem. Soc. 115 (1993) 3448.
[14] J. Bolger, A. Gourdon, E. Ishow, J.P. Launay, Inorg. Chem. 35 (1996) 2937.
[15] B.P. Sullivan, D.J. Salmon, T.J. Meyer, Inorg. Chem. 17 (1978) 3334.
[16] E. Alessio, Chem. Rev. 104 (2004) 4203.
[17] E. Alessio, G. Mestroni, G. Nardin, W.M. Attia, M. Calligaris, G. Sava, S. Zorzet, Inorg. Chem. 27 (1988) 4099.
[18] R. Ziessel, V. Grosshenny, M. Hissler, C. Stroh, Inorg. Chem. 43 (2004) 4262.
[19] J.S. Jaswal, S.J. Rettig, B.R. James, Can. J. Chem.-Rev. Can. Chim. 68 (1990) 1808.
[20] M. Calligaris, Coord. Chem. Rev. 248 (2004) 351.
[21] J.A. Davies, The coordination chemistry of sulfoxides with transition metals, in: H.J. Emeléus, A.G. Sharpe (Eds.), Advances in Inorganic Chemistry, Academic Press, 1981, pp. 115–187.
[22] E. Ishow, A. Gourdon, J.P. Launay, P. Lecante, M. Verelst, C. Chiorboli, F. Scandola, C.A. Bignozzi, Inorg. Chem. 37 (1998) 3603.
[23] S. Bodige, A.S. Torres, D.J. Maloney, D. Tate, G.R. Kinsel, A.K. Walker, F.M. MacDonnell, J. Am. Chem. Soc. 119 (1997) 10364.
[24] T. Norrby, A. Borje, A. Akermark, L. Hammarstrom, J. Alsins, K. Lashgari, R. Norrestam, J. Martensson, G. Stenhagen, Inorg. Chem. 36 (1997) 5850.
[25] E. Ishow, A. Gourdon, J.P. Launay, C. Chiorboli, F. Scandola, Inorg. Chem. 38 (1999) 1504.